대한방사선종양학회지 2010;28(4):224~230 DOI: 10.3857/jkstro.2010.28.4.224

# Evaluation of Scatter Reduction Effect of the Aft-Multiple-Slit (AMS) System Using MC Simulation

Jina Chang, M.S.*, Tae-Suk Suh, Ph.D.*, Doh-Yun Jang, M.S.†, Hong-Seok Jang, M.D.‡ and Siyong Kim, Ph.D.§

*Department of Biomedical Engineering, The Catholic University of Korea School of Medicine, †Department of Nuclear Engineering, Hanyang University, ‡Department of Radiation Oncology, Seoul St.Mary's Hospital, The Catholic University of Korea School of Medicine, Seoul, Korea, §Department of Radiation Oncology, Mayo Clinic, Jacksonville, FL, USA

Purpose: We designed the aft-multiple-slit (AMS) system to reduce scatter in cone-beam computed tomography (CBCT). As a preliminary study, we performed a Monte Carlo N-Particle Transport Code (MCNP) simulation to verify the effectiveness of this system.

Materials and Methods: The MCNPX code was used to build the AMS geometry. An AMS is an equi-angled arc to consider beam divergence. The scatter-reduced projection images were compared with the primary images only and the primary plus scatter radiation images with and without AMS to evaluate the effectiveness of scatter reduction. To obtain the full 2 dimensional (2D) projection image, the whole AMS system was moved to obtain closed septa of the AMS after the first image acquisition.

Results: The primary radiation with and without AMS is identical to all the slit widths, but the profiles of the primary plus scattered radiation varied according to the slit widths in the 2D projection image. The average scatter reduction factors were 29%, 15%, 9%, and 8% when the slit widths were 5 mm, 10 mm, 15 mm, and 20 mm, respectively.

Conclusion: We have evaluated the scatter reduction effect of the AMS in CBCT imaging using the Monte Carlo (MC) simulations. A preliminary study based on the MCNP simulations showed a mount of scatter reduction with the proposed system.

Key Words: Aft-multiple-slit (AMS), Scatter reduction, Cone-beam CT (BCT)

## Introduction

A cone-beam computed tomography (CBCT) has been widely used for the purpose of image-guided radiation therapy. This image-guidance is an important development for precise treatment dose delivery[1~3] and is being introduced for clinical applications, such as adaptive radiation therapy.[4,5] CBCT imaging systems employ a conventional X-ray tube and flat panel detector, and this system provides both 2 dimensional (2D) radiographs and CBCT for target localization. However, the presence of scattered radiation due to the large projection field size reduces the contrast, increases the image noise, and generates artifacts in reconstructed 3D images.[6,7]

Numerous strategies for scatter correction and rejection methods have been reported. The compensation filter[8,9] is known as a bowtie filter, and is used for reduction of scatter and patient dose. The X-ray beam is modulated to compensate for variation of patient attenuation using this system. The scatter correction algorithm,[10,11] which adopts pre-acquired 2D scatter fluence, was used to estimate scatter effect, then applied to each projection in CBCT to reduce a scattering. The most practical methods are air gap or/and anti-scatter grids.[12~14] By increasing the distance between patient and detector and using grids, a fair amount of scatter radiation can be reduced. However, there are some limitations, such as increased patient dose due to an attenuation of primary beam, the focal spot blurring effect, and reduced field of view in the

Submitted June 4, 2010, accepted October 20, 2010
Reprint requests to Tae-Suk Suh, Ph.D., Department of Biomedical Engineering, The Catholic University of Korea School of Medicine, 505 Banpo-dong, Seocho-gu, Seoul 137-701, Korea
Tel: 02)2258-7232, Fax: 02)2258-7506
E-mail: suhsanta@catholic.ac.kr

air gap method. The slot scan method[15~17] employing single or multiple narrow fan beams can be used for scatter reduction without attenuation of primary x-rays. However, it requires accurate synchronization of the fore-and aft-silts.

In this approach, we propose a new aft-multiple-slit (AMS) system for reduction of scattering in CBCT. The AMS with equi-angled intervals prevents scatter radiation in a longitudinal direction, and this whole AMS system moves after one gantry rotation. The projection images were reconstructed using a CBCT image reconstruction method. As a preliminary study, we performed the Monte Carlo N-Particle Transport Code (MCNP) simulation to verify the effectiveness of this system.

## Materials and Methods

### 1. MCNPX geometry and simulation set-up

The MCNPX program (v2.5d3, Los Alamos National Laboratory, Los Alamos, NM, USA) with the standard library of MCPLIB04 was used to build the imaging geometry of the AMS and obtain 2D projection images. The MCNPX radiography tallies (PI, TIR, and TIC), which are based on point detector, were used to evaluate an effect of scatter reduction in CBCT. The radiography grid is an array of point detectors placed close enough to each another so as to generate an image based on each point detector flux. We used a TIR radiography tally associated with flux image radiography on a planar image surface, and we obtained the only scattered radiation and scattered plus primary radiation separately using this tally option. By the asterisk flagging of this tally type we can change the units from particle flux (particles/cm$^2$) to energy flux (MeV/cm$^2$).

Fig. 1 shows the geometry of the AMS system. This system is an equi-angled arc to consider beam divergence. Although the AMS moves duringgantry rotation, the beam divergence still remains identical. The photon energy is 40 kVp mono-energy, and the source-isocenter distance is 100 cm and source-detector distance is 130 cm. The cylindrical water phantom model of 20 cm diameter includes polyvinyl chloride (1.406 g/cm$^3$) of 4 cm, polyurethane (0.021 g/cm$^3$) of 6 cm, and polytetrafluoroethylene (Teflon; 2.25 g/cm$^3$) of 12 cm diameter cylinder. The detector size is 30×30 cm (128×128 pixels), and a pixel size is 2.34×2.34 mm. The widths of the AMS were changed from 5 mm to 20 mm in 5 mm increments, and the depth of the AMS was 10 mm.

### 2. Evaluation of scatter reduction

We evaluated the effect of AMS by comparing with the primary and scatter radiation without AMS. The 2D projection of the phantom with AMS was generated by the sum of 2

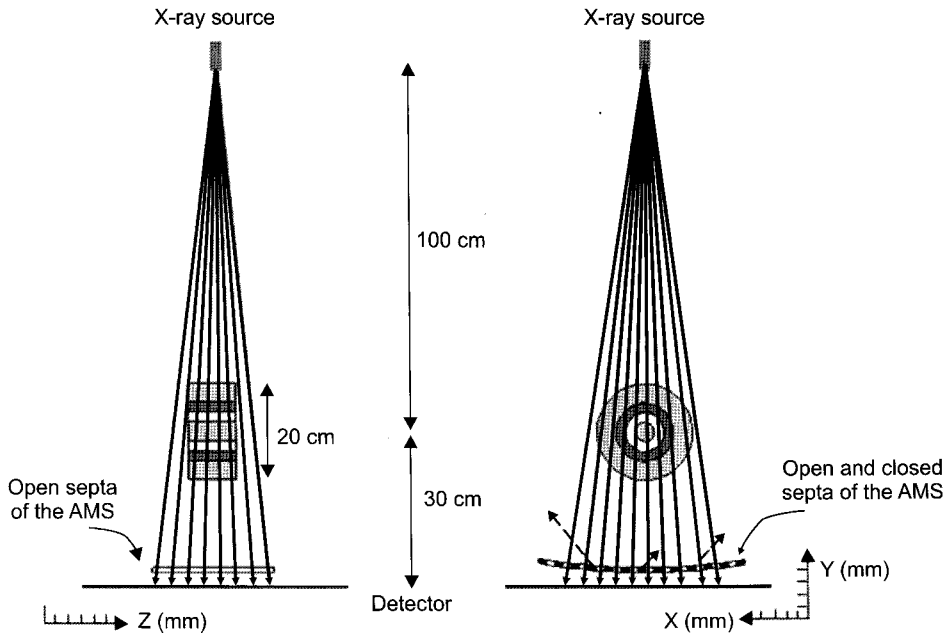


**Fig. 1.** The geometry of the aft-multiple-slit (AMS) system.

projection views (one with the original AMS view and the other with opposite view of the original AMS view). The profile along the x-axis of the phantom at the center was calculated to evaluate the scatter reduction of the 2D radiograph at each slit width.

The scatter-to-primary ratio (SPR) is defined as the ratio of scattered-to-primary radiation. The primary radiation was calculated by subtracting the scattered only calculation result from the scatter plus primary result of the MCNPX. The SPR profile along the x-axis of the phantom at the center was calculated to evaluate the scatter reduction of the 2D radiograph at each slit width.

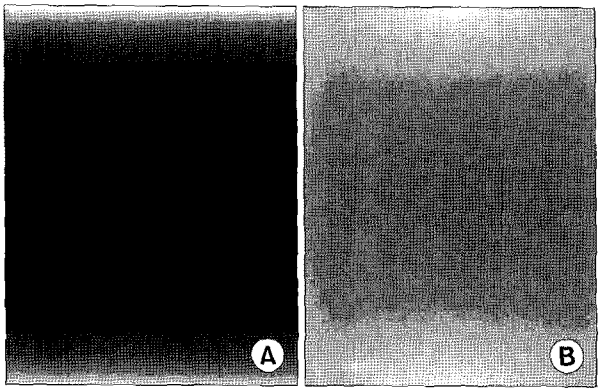


**Fig. 2.** The projection image with (A) the scattered and primary radiation, and with (B) the scattered only radiation of the phantom.

Scatter reduction factor (SRF) is used to quantify the effect of scattered reduction directly of the AMS system, and the SRF can be defined as follows:

$$SRF = \frac{S^{WO} - S^{MS}}{S^{WO}} \quad (1)$$

$S^{WO}$ and $S^{MS}$ are scattered radiation with and without AMS.

## 3. CBCT reconstruction

Theoretically, the slits were move totally opposite side after one gantry rotation, then another one more rotation, projection images were obtained by sum two radiographs at each angle. For a CBCT reconstruction we copy a radiograph at each angle, because the cylindrical phantom was designed symmetrically. Total 360 projections were used to reconstruct CBCT

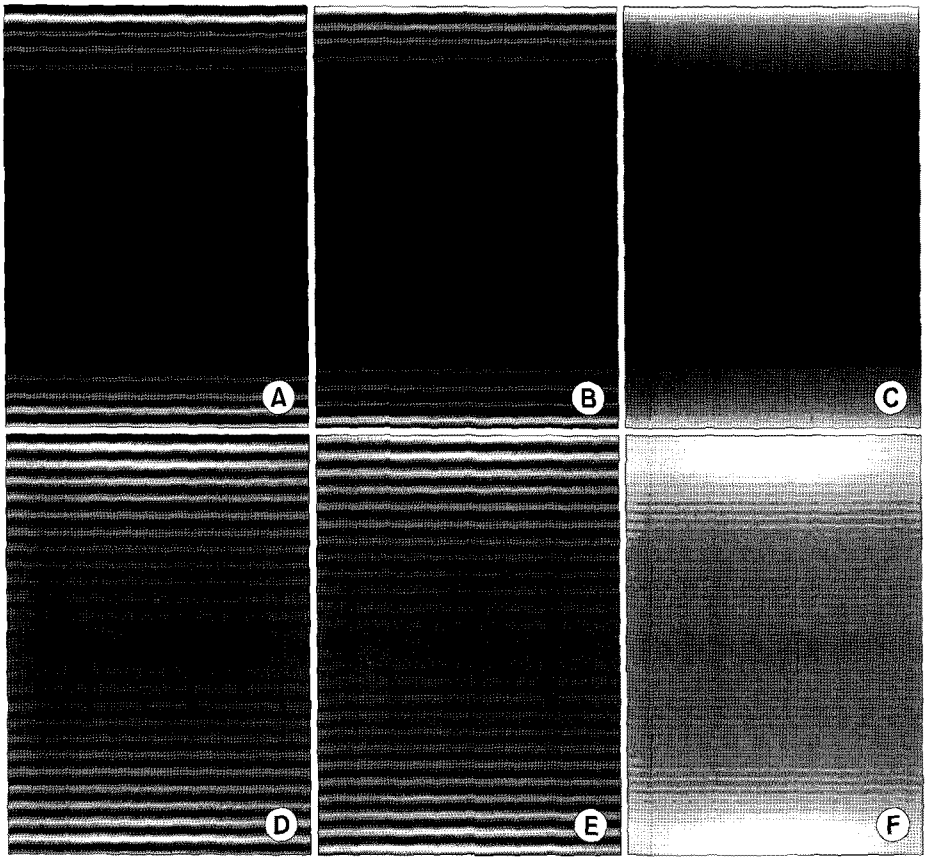


**Fig. 3.** The projection images of the scattered and primary radiation with (A) the 5 mm width aft-multiple-slit (AMS), (B) the opposite view after the second gantry rotation, (C) their summation view of the (A) and (B), and the projection images of the scattered only radiation with (D) the 5 mm width AMS, (E) the opposite view after the second gantry rotation, (F) their summation view of the (D) and (E).

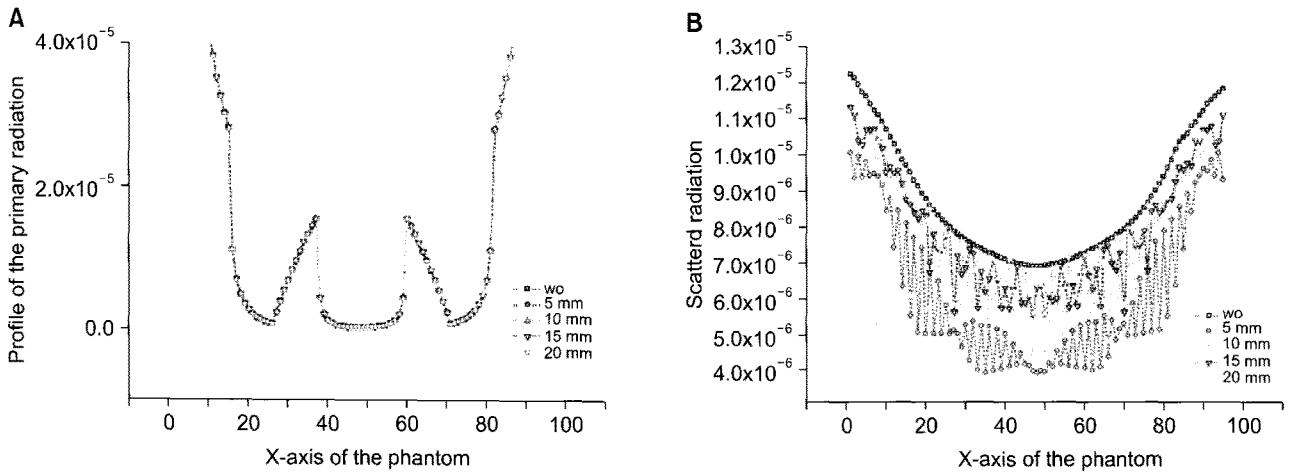


**Fig. 4.** The x-axis phantom profiles of (A) the primary radiation, and (B) scattered only radiation with/without (wo) the aft-multiple-slit system.

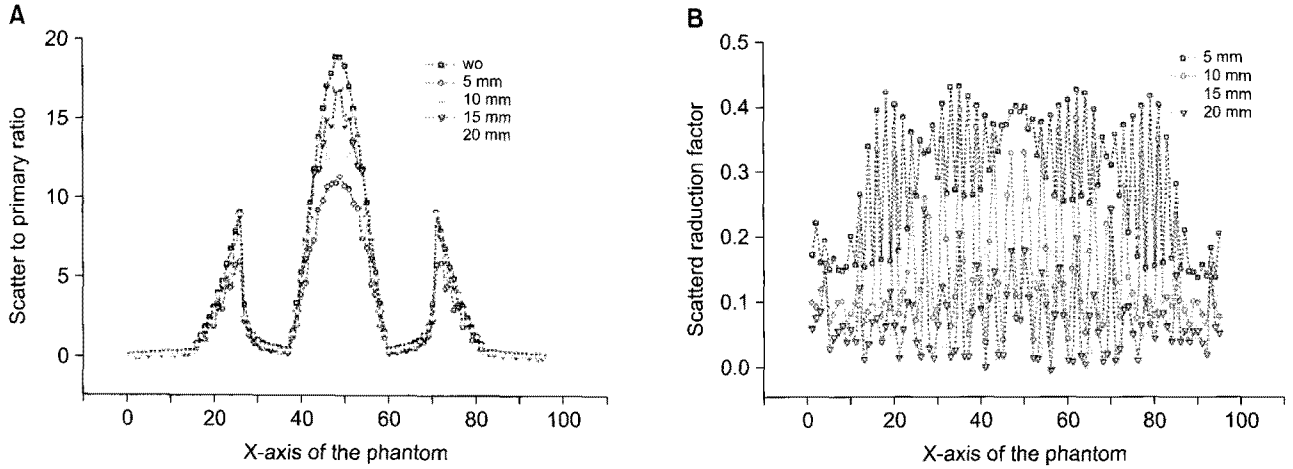


**Fig. 5.** (A) The scatter primary ratio and (B) the scatter reduction factor of the aft-multiple-slit system.

image. Then we compared line intensity profiles with CBCT reconstruction image of primary radiation only image. A reconstructionmechanism, based on the Feldkamp, Davis, and Kress (FDK) reconstruction algorithm,[18] was used to reconstruct the CBCT images, and software was written in Matlab 7.0.

**Table 1. The Maximum, Minimum, and Average Scatter Reduction Factor (SRF) at Each Different Aft-Multiple-Slit Widths**

| | 5 mm | 10 mm | 15 mm | 20 mm |
|---|---|---|---|---|
| Maximum SRF | 0.432 | 0.395 | 0.273 | 0.243 |
| Minimum SRF | 0.135 | 0.036 | 0.003 | −0.007 |
| Average SRF | 0.285 | 0.150 | 0.093 | 0.069 |

## Results

Fig. 2A shows the projection image with the scattered and primary radiation. Fig. 2B shows the projection image with the scattered only radiation of the phantom. When the AMS system is placed in the MCNP geometry, we obtained two projection images. Fig. 3A shows the projection images of scattered and primary radiation with the 5-mm width AMS during the first gantry rotation and Fig. 3B shows the opposite view after the second gantry rotation. By summation of the two images of 3A and 3B, we obtained Fig. 3C. Fig. 3D shows the projection images of the scattered only radiation with the 5-mm width AMS, Fig. 3E shows the opposite view

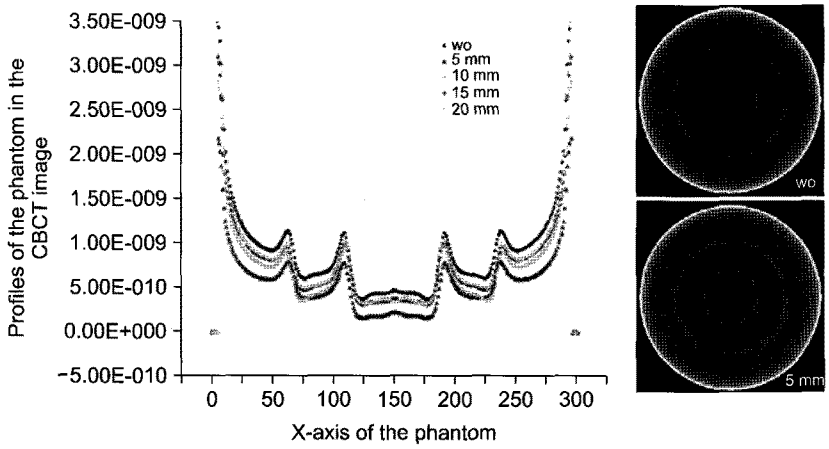


**Fig. 6.** The x-axis profiles and reconstructed cone-beam computed tomography (CBCT) image of the phantom with/without the aft-multiple-slit system.

after the second gantry rotation, and Fig. 3F shows the summation view of Fig. 3D and 3E. We can see the shadow regions of the AMS in each image.

Fig. 4A shows the x-axis phantom profiles of primary radiation, and Fig. 4B shows the x-axis phantom profiles of the scattered only radiation with and without the AMS. As can be seen, the primary radiation is identical in all the slit widths and without AMS, but the profiles of scattered radiation were changed according to the slit widths.

Fig. 5A and B show the SPR and SRF of the AMS system. As can be seen, the use of thinner AMS width could reduce the SPR values, and raise the SRF values. Table 1 shows the maximum, minimum, and average SRF at different AMS widths. The maximum SRFs were 43%, 40%, 27%, and 24%, and the average SRPs were 29%, 15%, 9%, and 8% when the slit widths were 5 mm, 10 mm, 15 mm, and 20 mm, respectively. The minimum SPF of the 20-mm slit width shows a negative value which was considered the noise value. Intuitively, it is considered the smaller the width, the better the effect of scatter reduction is, although it requires a greater burden in engineering precision. Fig. 6 shows the x-axis profiles and reconstructed CBCT image of the phantom with and without AMS. The profiles of the 10 mm, 15 mm, and 20 mm slit widths were almost identical in the center area of the image, but the profiles changes towards the periphery area of the image similar to the 2D projection image.

## Discussion

The typical dynamic slit scan system consists of for- and aft-slit collimators, and is required for accurate synchronization. However, the design of our system requires simple hardware configuration of static AMS, and can be easily adapted to conventional systems. Moreover, there is no need for the additional scatter reduction process. We believe that the scatter reduction rate could be increased more in conjunction with the anti-scatter grid of the imaging detector.

However, a relatively long scan time could degrade the image quality due to patient motion, and there could be discontinuities between two projection images in a real environment. Imaging dose to the patient also could be a problem. In this system, the patient dose is expected to be twice as large as the conventional scanning system.

Considering that typical kVp value in CBCT ranges from 100 kVp to 125 kVp, we chose 40 keV mono-energy photons in this study. Scatter radiation is produced mainly when Compton scattering interactions occur and the Compton scattering cross-section of water (or tissue) is higher with higher photon energy in the range of the CBCT X-ray. Because we are considering the scatter reduction effect, it would be more conservative to take the lower side of photon energy.

A further study will be investigated by changing the AMS position or combination with a for- multiple-slit system to increase the scatter reduction effect and reduce the patient doses.

In conclusion, CBCT imaging provides useful volumetric anatomy information for patient set-up and adaptive radiation therapy, and the imaging quality can be improved by reducing scattered radiation. In this study, we have evaluated the scatter reduction effect of the AMS system in CBCT imaging. A

preliminary study based on the MCNP simulations showed a significant scatter reduction effect. Our system could be a useful solution to improve the image quality and dose calculation accuracy in CBCT imaging.

## Acknowledgements

This research was sponsored by the National Research Foundation of the Ministry of Education, Science and Technology of Korea (2010-0003315, K20901000001-09E0100-00110).

## References

1. **Jaffray DA, Siewerdsen JH, Wong JW, Martinez AA.** Flat-panel cone-beam computed tomography for image-guided radiation therapy. Int J Radiat Oncol Biol Phys 2002;53:1337-1349
2. **Hawkins MA, Brock KK, Eccles C, Moseley D, Jaffray D, Dawson LA.** Assessment of residual error in liver position using kV cone-beam computed tomography for liver cancer high-precision radiation therapy. Int J Radiat Oncol Biol Phys 2006;66:610-619
3. **Thilmann C, Nill S, Tucking T, et al.** Correction of patient positioning errors based on in-line cone beam CTs: clinical implementation and first experiences. Radiat Oncol 2006;1:16
4. **Langen KM, Meeks SL, Poole DO, et al.** The use of megavoltage CT (MVCT) images for dose recomputations. Phys Med Biol 2005;50:4259-4276
5. **Samant SS, Xia J, Muyan-Ozcelik P, Owens JD.** High performance computing for deformable image registration: towards a new paradigm in adaptive radiotherapy. Med Phys 2008;35:3546-3553
6. **Yang Y, Schreibmann E, Li T, Wang C, Xing L.** Evaluation of on-board kV cone beam CT (CBCT)-based dose calculation. Phys Med Biol 2007;52:685-705
7. **Morin O, Chen J, Aubin M, et al.** Dose calculation using megavoltage cone-beam CT. Int J Radiat Oncol Biol Phys 2007;67:1201-1210
8. **Tkaczyk JE, Du Y, Walter D, Wu X, Li J, Toth T.** Simulation of CT dose and contrast-to-noise as a function of bowtie shape. Proc SPIE 2004;5368:403-410
9. **Mail N, Moseley DJ, Siewerdsen JH, Jaffray DA.** The influence of bowtie filtration on cone-beam CT image quality. Med Phys 2009;36:22-32
10. **Ning R, Tang X, Conover D.** X-ray scatter correction algorithm for cone beam CT imaging. Med Phys 2004;31:1195-1202
11. **Siewerdsen JH, Daly MJ, Bakhtiar B, et al.** A simple, direct method for x-ray scatter estimation and correction in digital radiography and cone-beam CT. Med Phys 2006;33:187-197
12. **Shaw CC, Wang T, Gur D.** Effectiveness of antiscatter grids in digital radiography. A phantom study. Invest Radiol 1994;29:636-642
13. **Neitzel U.** Grids or air gaps for scatter reduction in digital radiography: a model calculation. Med Phys 1992;19:475-481
14. **Lui X, Shaw CC.** Effects of anti-scatter grid on measurement of detector characteristics. Med Phys 2002;29:1342
15. **Jing Z, Huda W, Walker JK.** Scattered radiation in scanning slot mammography. Med Phys 1998;25:1111-1117
16. **Mainprize JG, Ford NL, Yin S, Tumer T, Yaffe MJ.** A slot-scanned photodiode-array/CCD hybrid detector for digital mammography. Med Phys 2002;29:214-225
17. **Samei E, Saunders RS, Lo JY, et al.** Fundamental imaging characteristics of a slot-scan digital chest radiographic system. Med Phys 2004;31:2687-2698
18. **Feldkamp LA, Davis LC, Kress JW.** Practical cone-beam algorithm. J Opt Soc Am 1984;1:612-619

대한방사선종양학회지 2010;28(4):224~230

국문초록

# MC 시뮬레이션을 이용한 Aft-Multiple-Silt 시스템의 산란선 제거 효과 평가

가톨릭대학교 의과대학 의공학교실*, 한양대학교 원자력공학과†, 가톨릭대학교 서울성모병원 방사선종양학과‡, Mayo Clinic 방사선종양학과§

장지나* · 서태석* · 장도윤† · 장홍석‡ · 김시용§

**목 적:** 본 연구에서는 콘빔 CT에서 산란선 제거를 위한 aft-multple-slit (AMS) 시스템을 설계하였다. 예비 연구로서 본 시스템의 효용성을 검증하기 위해 MC 시뮬레이션을 수행하였다.

**대상 및 방법:** 가상 시뮬레이션은 산란선과 산란선+일차선을 계산할 수 있는 MCNPX의 radiography tally 5를 이용하였다. AMS는 빔의 발산성을 고려한 각이 동일한 아크 형태이고, 길이 방향에서의 산란선을 막는다. AMS의 효용성을 위한 평가는 AMS를 사용하지 않았을 때의 일차선과 산란선을 비교함으로써 수행되었다. 2D projection 영상을 얻기 위해 전체의 AMS는 한번의 갠트리 회전 후 AMS에 의해 가려진 부분의 영상 획득을 위해 다시 한 번 회전하는 구조이다.

**결 과:** 일차선의 2D projection 영상은 모든 AMS의 폭에서 그리고 AMS를 사용하지 않았을 때에도 동일하였으나 일차선+산란선의 2D projection 영상은 slit의 폭에 따라 결과가 변했다. Slit의 폭을 5 mm, 10 mm, 15 mm, 20 mm로 하였을 때 평균 산란성 제거율은 29%, 15%, 9%, 8%였다.

**결 론:** 본 연구에서는 AMS를 이용한 콘빔 CT의 산란선 제거 효과를 평가하였다. MC 시뮬레이션을 이용한 본 시스템의 사전 연구에서는 상당한 산란선 제거 효과를 보여주었다.

**핵심용어:** Aft-multiple-slit, 산란선 제거, 콘빔 CT